International Journal of Heat and Mass Transfer 139 (2019) 873–880

Contents lists available at ScienceDirect

International Journal of Heat and Mass Transfer

journal homepage: www.elsevier.com/locate/ijhmt

Decomposition by film boiling heat transfer of glycerol

Pushan Sharma [a], C. Thomas Avedisian [a,*], Jordan D. Brunson [a], Wing Tsang [b]

[a] Sibley School of Mechanical and Aerospace Engineering, Cornell University, Ithaca, NY 14853, USA
[b] Physical and Chemical Properties Division, National Institute of Standards and Technology, Gaithersburg, MD 20899, USA

ARTICLE INFO

Article history:
Received 12 December 2018
Received in revised form 10 April 2019
Accepted 2 May 2019
Available online 29 May 2019

Keywords:
Boiling
Glycerol
Film boiling
Critical heat flux
CHF
Decomposition
Synthesis gas
Biodiesel
Pyrolysis

ABSTRACT

In this paper, a simple method is presented to transform saturated liquid glycerol into a gaseous fuel mixture containing hydrogen (H_2), carbon monoxide (CO), methane (CH_4), ethylene (C_2H_4), and ethane (C_2H_6). It is based on glycerol decomposition within the vapor film of the film boiling regime of multiphase heat transfer on a horizontal tube. In film boiling, a thin gas layer of predominantly glycerol vapor surrounds the tube and decomposes as the gases flow in the film under the influence of buoyancy. The decomposition products are removed in the form of bubbles percolating through the liquid pool and their contents are chemically analyzed to determine the decomposition products and their fractional amounts.

The glycerol boiling curve and critical heat flux were measured to determine the operational domain for decomposition which is between glycerol's minimum film boiling temperature and an upper value dictated by material considerations of the tube that supports the vapor film. The results show that 95% of the gases produced by decomposition of glycerol are themselves viable as a fuel. Decomposition of glycerol is a multistep process initiated by radical species in the product stream. Key reactions are identified by a sensitivity and pathway analysis. An optimal thermal efficiency and corresponding temperature for conversion corresponding to the experimental design is suggested for conversion by film boiling at atmospheric pressure.

© 2019 Elsevier Ltd. All rights reserved.

1. Introduction

Glycerol ($C_3H_8O_3$, boiling point of 563 K) is a waste product from the manufacture of biodiesel. So much of it is now produced that there is a surplus of glycerol which can threaten the biodiesel industry [1–5]. Glycerol may be burned directly [6–12] or reformed into other combustible gases using various stationary reactor designs [13–23]. In this paper, we discuss a new approach for reforming glycerol into a mixture of combustible gases. The idea is to boil it.

The particular regime of boiling heat transfer that is most conducive to affecting chemical change of an organic molecule is film boiling. Fig. 1 is a schematic of this boiling regime as it relates to a horizontal tube in a bulk liquid in a gravitational field 'g'. A cross-sectional schematic viewed along the axis of the tube where bubbles form is shown. In many applications such as nuclear safety and electronic cooling, among others, process variables are adjusted to avoid this heat transfer mode because of the potential to damage the surface on which the vapor film forms. However, under well-controlled conditions, it can provide a thermal environment conducive to decomposing a molecule for a useful purpose, such as reforming a chemical into alternative substances. Recent work has shown this capability [24,25].

In this study, we use film boiling to transform glycerol into a gaseous mixture with potential for use as a fuel. The surface configuration employed is a horizontal metal tube, though other geometries can be used. The tube is submerged in a stagnant pool of glycerol and then electrically heated to boil glycerol and transition the multiphase heat transfer regime into film boiling. The gases in the vapor film decompose and collect in bubbles that form at the top of the tube. The decomposition products are transported by buoyancy through the liquid away from the tube. They are then analyzed to determine the gas composition and fractional amounts of species formed. In the variant presented here, gases transported out of the pool are not allowed to reflux so that the pool remains pure throughout operation. Results can thus be interpreted solely in terms of glycerol decomposition.

Advantages of film boiling for promoting decomposition of glycerol are as follows: the reactor space is developed in a self-assembled manner and does not need to be fabricated in the traditional sense; buoyancy alone is sufficient to transport the reactant gases in the vapor film thus no pumps are required; vaporization of glycerol and transport of the vapors produced into

* Corresponding author.
E-mail address: cta2@cornell.edu (C.T. Avedisian).

https://doi.org/10.1016/j.ijheatmasstransfer.2019.05.005
0017-9310/© 2019 Elsevier Ltd. All rights reserved.

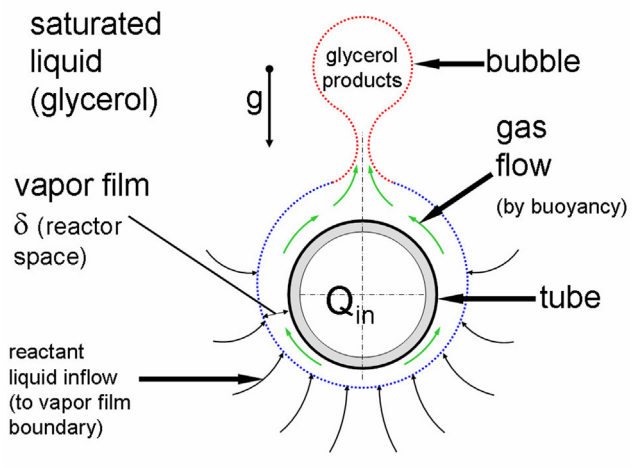

Fig. 1. Schematic of film boiling on a horizontal tube.

the reactor space are coupled processes so separate vaporizers are not needed; the simplicity of this concept makes it portable.

The temperature range of the experiments reported here is from 1250 K to 1550 K. The highest prior reported temperature for glycerol decomposition appears to be 1073 K in a flow tube [14]. Higher temperature data are important for pyrolysis reactions relevant to oxidative processes that typically operate at higher temperatures.

As a first consideration for decomposing glycerol the unimolecular reaction [21] is noted,[1]

$$C_3H_8O_3 \rightarrow 3CO + 4H_2 \qquad (R1)$$

The product gases in this case are hydrogen (H_2) and carbon monoxide (CO) in the molar ratio of 4/3. In reality, other products including radicals may be present as postulated here to explain the results presented.

Section 2 describes the experimental design and operation followed by a discussion in Section 3 of the experimental results where a detailed analysis of the reaction pathways is included to explain the formation of the stable species detected. Section 4 analyzes the results in terms of a thermal efficiency for decomposing glycerol, and an optimal operating condition is suggested.

2. Experiment

2.1. Design

Fig. 2 is a schematic of the apparatus. It employs a 4L glass cylinder filled with 3.5L of glycerol and closed at its ends with metal flanges sealed with high temperature-resistant o-rings (DuPont Kalrez 7075). Four 300W immersion heaters maintain the bulk glycerol at near saturation. A horizontal metal tube (Inconel 600) serves as a resistance heater. The tube is supported at each end by copper electrodes and is suspended in the chamber by electrically isolated feed-through fittings in the upper metal flange. An electric current is passed through the electrodes and tube to heat the tube and fluid in contact with it to transition the heat transfer modes into film boiling.

During film boiling, bubbles form at the top of the tube. The bubbles contain the decomposition products at compositions that are fixed as the bubbles percolate through the relatively colder liquid. At the free liquid surface, the gases are released and pass out of the system where they flow through condensers, vapor traps, and a flow meter. The gases are analyzed by gas chromatography (GC) analysis to identify the stable species formed and their fractional amounts in the gaseous mixture. Additional details of the apparatus may are given in [24,25].

In the particular configuration of Fig. 2, all condensable species from decomposition along with unreacted glycerol flow out of the reaction chamber; however, only glycerol is refluxed back into the chamber. Fig. 3 is a schematic of the flow paths. In this way, all species detected are attributed entirely to glycerol decomposition. The liquid pool was periodically sampled and analyzed (i.e., by 1D 1H and 13C NMR spectroscopy) and showed only trace quantities of impurities. By preventing refluxing of non-glycerol condensables and maintaining the chamber with pure glycerol it was easier to trace the origin of the product gases to the decomposition of glycerol. Since all gases generated are due to glycerol decomposing, and all such gases pass through the flow meter, a zero flow rate would be indicative of no decomposition.

The heater tube is made of a polished nickel alloy (Inconel 600, Microgroup Inc., #600F10125X028SL, 1686 K melting point) with a ceramic tube insert for structural integrity. The tube dimensions were 3.175 mm O.D. (D_o), 1.753 mm I.D. (D_i), and 80 mm long (L). The active heating length is the central 60 mm portion of the tube. Two thermocouples (Omega, SCAXL-020G) are positioned inside the ceramic tube and spaced 20 mm from the copper electrode clamps. The tube temperature is taken as the average of the two recorded temperatures.

The heat flux to the tube is determined by the electrical power per surface area, $I^2 R/A_s$, where resistance $R = \rho L/A_x$, ρ is the resistivity of Inconel 600, $L = 60$ mm is the active length of the tube, A_x is the tube cross-sectional area $\left(\pi\left(D_o^2 - D_i^2\right)/4\right)$, and A_s is the tube surface area ($\pi D_o L$). The resistivity was related to temperature up to 1200 K [24] with extrapolations to higher temperature based on a linear fit to the available data.

2.2. Creating film boiling and measuring product gases

The process of developing film boiling here involved immersing the tube into a pool of nearly saturated glycerol and (Joule) heating the tube to force a transition of the heat transfer modes from single phase convection, nucleate boiling, critical heat flux (CHF), and film boiling. The transition to film boiling for glycerol was found to be similar to ethanol and diethyl carbonate as previously reported [24,25] where videos showing the transitions are included. Increasing heat flux beyond the CHF point results in a tube temperature increase from about 600 K to 1530 K. The initiation of film boiling was found to occur randomly along the tube – at the left end, center, or right end of the tube.

Once in the film boiling regime, the temperature was varied by adjusting the DC power input in 0.1 V increments (Agilent 6681A, 0–8 V, 0–580A with a PC interface (National Instruments, NI PCI-6281) under LabVIEW control). At each step, the product gas compositions were measured by directing a small amount of the exhaust gases (30 mL/min) into the GC (Gow-Mac Instruments, Series 600-TCD). The GC was controlled by Chromperfect software to obtain chromatograms indicating the mole fractions of distinct species at different reaction temperatures. Further details of the GC analysis are given in Appendix B. Thermal conditions were allowed to stabilize for 5 min before each GC sampling.

A thin carbon layer was found to form on the tube over time due to surface reactions. Tubes were weighed before and after each experiment (typically lasting several hours) to determine the mass of carbon formed from surface reactions. The amount was negligible compared to the carbon carried by non-condensable products. A carbon balance was inaccessible because carbon input to the

[1] Equation numbers are preceded by an 'R' when they represent a reaction.

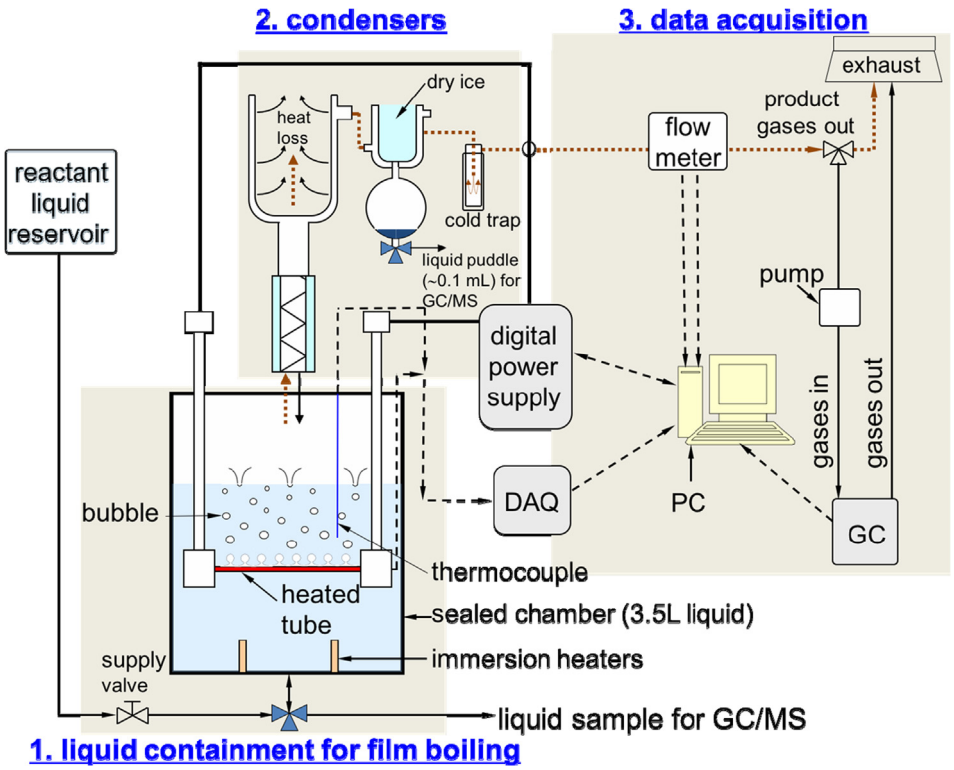

Fig. 2. Experimental layout: The sealed chamber contains only pure glycerol during operation. The brown dotted arrow indicates the flow path of gaseous products from the 4L cylindrical chamber to exhaust.

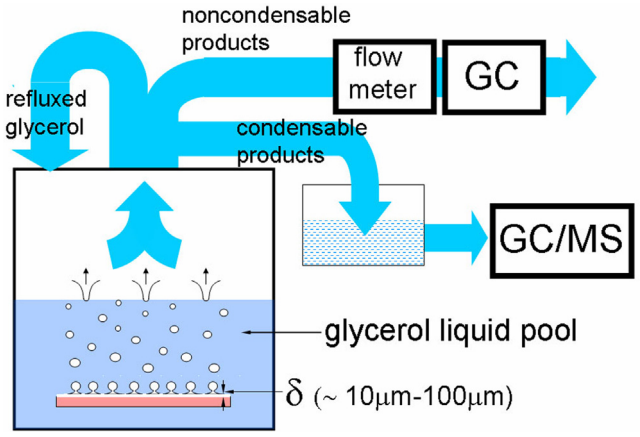

Fig. 3. Flow paths for the schematic of Fig. 2. Only glycerol is refluxed while other decomposition products (condensable and noncondensable) pass out of the chamber.

reactor space occursvia evaporation and it is not possible to directly measure the evaporation rate.

2.3. Experimental uncertainties

Experimental uncertainties are systematic as far as instrumentation accuracies and random with regard to experimental measurements. Most instrument uncertainties are negligible (e.g., power supply uncertainties are ±0.04% and ±0.1% in terms of voltage and current outputs, respectively). The systematic uncertainty for the K-type thermocouples used in the experiments is specified as 2.2 K or 0.75% of the measured value. Random temperature variations arise from fluctuations (≤10 K) about mean values (>1250 K) due to intermittent liquid/solid contact at the heated tube and from bubble departure cycles that draw in colder liquid as bubbles depart from the tube. For example, for a mean temperature of 1475 K the maximum uncertainty for temperature was 17 K or 1.1% of the mean temperature of 1475 K.

The flow meter (Omega #FMA-A2309) was calibrated against a standard meter (Bios International Corp. (Lakewood, CO), Definer 220). Results are given in Appendix A. The meter has a systematic uncertainty of ±1% of full scale. Flow rate uncertainties also contribute to uncertainties of the GC output of each species. These uncertainties will have the same relative magnitude compared to the uncertainties of the overall flow rate.

It is also noted that while there are significant temperature gradients across the vapor film in film boiling, the tube surface temperature can still be a reasonable measure of the reaction temperature based on a model presented in [24]. In the following discussions, the tube temperature is used as a reference thermal state with this consideration mind.

3. Results and discussion

3.1. Glycerol boiling curve, product yields, and flow rates

The boiling curve for glycerol is shown in Fig. 4. The film boiling regime is bounded at the lower end by T_2~1260K (the approximate minimum temperature below which a stable vapor film could not be maintained and the reactor space would disappear due to collapse of the vapor film) and at the upper end by T_3~1686K (Inconel's melting point). At approximately 1570 K the Inconel tubes showed signs of buckling.

The nucleate boiling regime terminates at the critical heat flux (CHF) which was measured for glycerol to be approximately 620 W/m^2 at temperature T_1. This value was within 15% of standard CHF correlations allowing for the finite size of the tube [26,27]. This difference is attributed to uncertainties in the

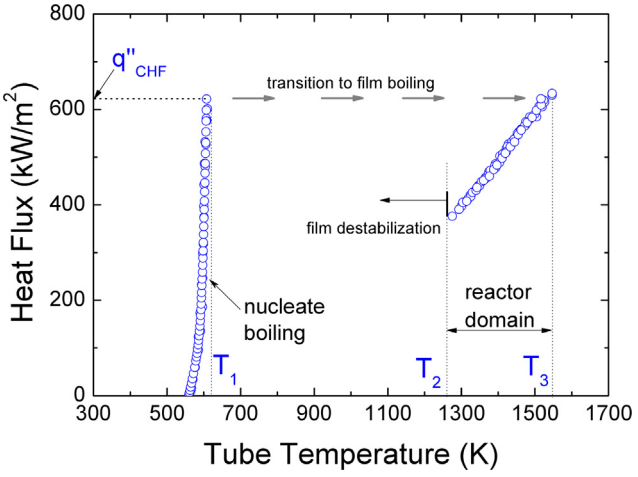

Fig. 4. Glycerol boiling curve.

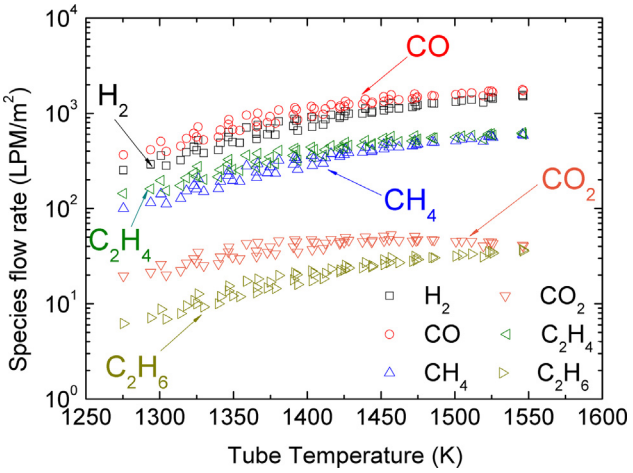

Fig. 6. Variation of individual stable species volumetric fluxes with average tube temperature.

empirical constants and thermo-physical properties required in the correlation. Correlations for the other boiling regimes are not as well established as CHF, so efforts were not undertaken to simulate them. After CHF, the boiling mode transitioned to film boiling with a concomitant temperature jump $T_1 \rightarrow T_3$. The $T_2 \leftrightarrow T_3$ range is the operational domain for thermal decomposition of glycerol.

Fig. 5 shows the variation of exhaust gas flow rate with temperature over the film boiling domain. The bars on the data represent ranges from fluctuations of the flow rate which are believed to have been caused by the aforementioned bubble departure cycles. The increase of flow rate with temperature is a consequence of the reaction rates of decomposition being strongly dependent on temperature. As the average gas temperature increases, the individual product species flow rates will increase along with the total gas flow rates as shown in Fig. 5.

Fig. 6 shows the variation of individual species volumetric fluxes with tube temperature. H_2 and CO have the highest volumetric fluxes, which is unsurprising considering that decomposition of glycerol has been shown to be a source of hydrogen [13–17]. Other gases (i.e., CO_2, CH_4, C_2H_4, and C_2H_6) are present in much smaller quantities which is consistent with other studies (e.g., which employed a tubular packed bed reactor with a catalyst [20]) and suggests that glycerol does not decompose entirely by

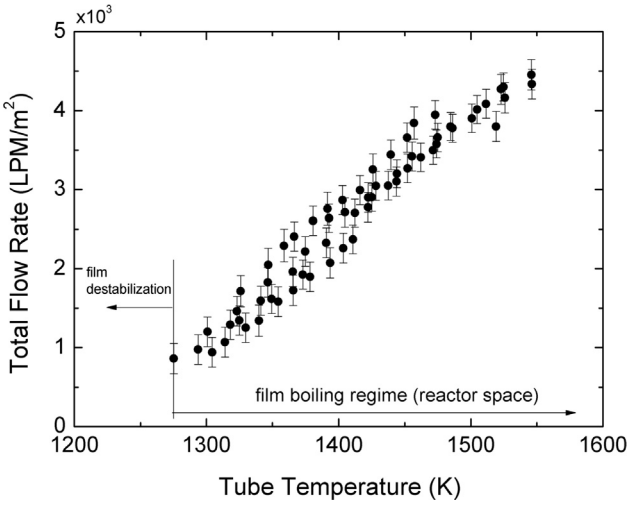

Fig. 5. Variation of total volumetric flux (Liters per minute per unit area) of exhaust gas with average tube temperature.

Table 1
Molar percentages of the product gases at selected temperatures.

Composition (mole%)	Temperature (K)		
	1320	1429	1517
H_2	31.4	31.7	35.1
CO	41.1	40.7	38.0
CH_4	10.0	12.1	12.0
C_2H_4	13.9	13.0	12.1
CO_2	3.2	1.8	1.9
C_2H_6	0.4	0.8	0.8
H_2 + CO	72.5	72.4	73.1

the simple unimolecular reaction (R1) under the conditions of the present study. This point is further discussed in Section 3.2.

Table 1 lists mole percentages of the species in Fig. 6 at three selected temperatures. The amount of syngas (H_2 + CO) in the product stream was just over 70% at all temperatures. Other decomposition technologies have shown syngas production from glycerol varying between 60% and 80%, though at lower temperatures [14,20,22]. For film boiling, the average gas temperature can be lower than the tube temperature [24] thus film boiling product yields may be more in line with the prior lower temperature studies. At the same time, methane and ethane production as seen in Table 1 are four and six higher times higher, respectively, than reported in [14]. Although the syngas yield is lower, the recoverable energy of the product gases (see Section 4), measured in terms of their heats of reaction, can be higher because of the formation of other high-value species.

3.2. Sensitivity and pathway analysis

The pathways for the formation of the product gases H_2, CO, C_2H_4, CH_4, CO_2 and C_2H_6 (Fig. 6) are discussed in this section. As noted in Section 2.1, the liquid pool remained essentially pure throughout operation because condensable, non-glycerol products were cycled out of the system. The pathways for glycerol decomposition are then due entirely to glycerol and not the decomposition of any preferentially vaporized condensables that may have been refluxed.

The process of validating the controlling reactions for decomposition typically requires the availability of a detailed numerical model for the reactor along with a chemical mechanism with known rate constants and a thermophysical property database as the starting point. Unfortunately, such information does not currently exist for film boiling that includes decomposition of the

gases flowing in the vapor film. The alternative is to look to other reactor configurations for insights on the controlling mechanisms with an expectation that what is relevant to one reactor may be applicable in a qualitative sense to the film boiling reactor. Although quantitative connections may not generally be possible between other reactor types (e.g., conventional tubular reactors) and film boiling because of differences in the way reactant gases are distributed in the system, we nonetheless selected the homogenous reactor configuration for this purpose because of the ability to predict the decomposition of organic molecules with ANSYS CHEMKIN® 18.0. In the following, we outline the main aspects of using this software for this reactor.

The matter to be addressed is that of identifying dominant reactions that lead to the production of stable species shown in Fig. 6. Pathway analysis can provide insights for this purpose. The detailed glycerol decomposition mechanism of [28] is the starting point. Fig. 7 summarizes the results of this analysis. The circled molecules are the stable species detected in the experiments (cf, Fig. 6), though radicals play a central role in glycerol decomposition as noted below. The following discussion provides a reaction set determined by quantitative means using pathway analysis. Details are omitted and only results of the pathway analysis carried out using ANSYS-CHEMKIN are discussed.

When exposed to elevated temperatures, there is an initial transient period of the glycerol decomposition process during which radical species form (e.g., H, OH). The radicals then attack glycerol and initiate decomposition. The pathway analysis suggests that the most important initiation reactions start with OH radical attack,

$$C_3H_8O_3 + OH \rightarrow C_3H_6O_2 + H_2O + OH \quad (R2)$$

At high temperatures (above 1400 K), the pathway analysis shows that glycerol may also decompose to form acetol,[2]

$$C_3H_8O_3 \rightarrow \text{acetol} + H_2O \quad (R3)$$

In an intermediate stage, the important species produced are acrolein (C_2H_3CHO), formaldehyde (HCHO) and acetaldehyde (CH_3CHO) (the latter two were detected in the liquid pool by NMR spectroscopy). Acrolein and water are produced by the dehydration reaction of $C_3H_6O_2$,

$$C_3H_6O_2 \rightarrow C_2H_3CHO + H_2O \quad (R4)$$

and acetol can also decompose to form acetaldehyde and formaldehyde,

$$\text{acetol} \rightarrow CH_3CHO + HCHO \quad (R5)$$

A final stage of decomposition involves reactions that eventually produce the stable species detected in the experiments. The H radical attack on acetaldehyde produces hydrogen and the intermediate radical CH_3CO,

$$CH_3CHO + H \rightarrow H_2 + CH_3CO \quad (R6)$$

CH_3CO may decompose to produce CO and the CH_3 radical

$$CH_3CO \rightarrow CH_3 + CO \quad (R7)$$

CH_3 can also react with OH radicals as

$$CH_3 + OH \rightarrow CH_3OH \quad (R8)$$

In (R8) we do not show a third body compound ('M') capable of chemical interaction with the reactant molecules for simplicity. Three-body collisions are themselves thought to be rare [29]. Reactions written as involving three bodies are symbolic for more steps that include the formation of activated intermediates. In what follows we chose not to show third body compounds in relevant reactions because this level of detail does not enhance the understanding of the pathways by which the stable compounds detected in the experiments form.

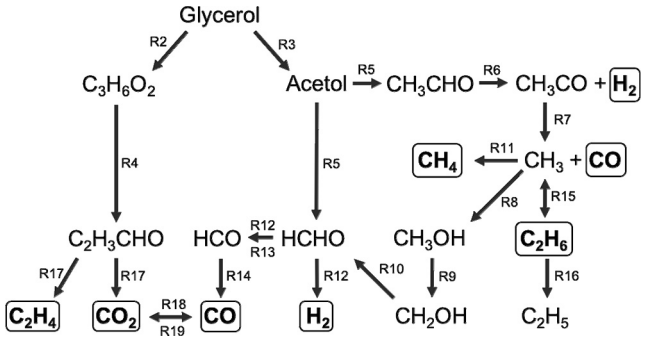

Fig. 7. Dominant routes for glycerol decomposition in film boiling as determined by pathway analysis. The measured stable species (Fig. 6) are encircled.

After (R8), OH attack on CH_3OH yields

$$CH_3OH + OH \rightarrow CH_2OH + H_2O \quad (R9)$$

CH_2OH decomposition will produce more formaldehyde,

$$CH_2OH \rightarrow HCHO + H \quad (R10)$$

The analysis shows that (R10) is a more important source of formaldehyde than (R5). Additionally, the pathway analysis shows that methane (CH_4) is formed by a three-body reaction (third-body not shown as noted above) as

$$CH_3 + H \rightarrow CH_4 \quad (R11)$$

The reaction with the highest impact on H_2 production involves H and OH atoms reacting with CH_2O,

$$HCHO + H \rightarrow H_2 + HCO \quad (R12)$$

while CH_2O can also react with OH,

$$HCHO + OH \rightarrow H_2O + HCO \quad (R13)$$

HCO was found to have the highest impact on CO production,

$$HCO \rightarrow H + CO \quad (R14)$$

The pathway analysis indicated that (R14) is more dominant than (R7) in the context of CO production.

Regarding ethane (C_2H_6), it can form and decompose via

$$CH_3 + CH_3 \rightleftharpoons C_2H_6 \quad (R15)$$

or

$$C_2H_6 + OH \rightarrow C_2H_5 + H_2O \quad (R16)$$

As shown in Fig. 6 the flow rate of ethane in the exhaust gas increases with temperature in spite of the opposing effect of (R15) and (R16). At low temperatures, the reaction pathway analysis shows that (R16) dominates (R15) and the flow rate of ethane is comparatively small in this regime as noted by the scale of Fig. 6. As temperature increases, the concentration of CH_3 increases resulting in a higher production rate of ethane through (R15) which increases the overall percentage of C_2H_6 in the gas stream, though the relative concentrations remain small.

As a final consideration, the source of CO_2 is considered to come from OH radical attack on acrolein

$$C_2H_3CHO + OH \rightarrow CO_2 + C_2H_4 + H \quad (R17)$$

Additional reactions for CO_2 production are the water gas shift reaction

[2] In the present paper 3-hydroxypropanal and 1-hydroxypropan-2-one are designated $C_3H_6O_2$ and CH_3COCH_2OH or "acetol", respectively.

$$CO + H_2O \rightarrow CO_2 + H_2 \quad \text{(R18)}$$

and

$$CO + OH \rightleftharpoons CO_2 + H \quad \text{(R19)}$$

which is a reversible reaction.

Pathway analysis showed that the forward reaction of (R19) (producing CO_2) is faster than the reverse reaction (consuming CO_2) at low temperature. As temperature increases, the reverse reaction was found to be important thus reducing the overall concentration of CO_2 which is consistent with the slight downturn of CO_2 concentration shown in Fig. 6 at high temperature. Based on the reaction rates (used in the homogeneous model), at low temperatures (R19) was found to be more important in producing CO than (R18) which depletes CO.

As previously noted, the reactions proposed above are developed in the context of a homogeneous reactor. Verification of decomposition processes for a film boiling reactor will require a detailed numerical model of film boiling that includes chemical change of the gases flowing in the film (an effort for future work).

4. Conversion efficiency

Flow reactors are typically used to develop gaseous products, determine reaction mechanisms, and verify rate constants when a detailed model of the reactor is available. Few considerations are given to the energetic requirements. For film boiling, it is useful to provide a measure of its effectiveness at chemical transformation because of its potential for scale-up to reform industrially relevant chemicals to alternative substances.

We define a film boiling 'transformation efficiency', ε, for conversion of an organic molecule as the energy that could be recovered from the gaseous products (W_P) divided by the energy input to the tube (Q_{in}):

$$\varepsilon = \frac{W_P}{Q_{in}} \quad (20)$$

We took W_P to be the sum of the lower heating values (LHV, ΔH_{ri}) of each stable species 'i' (see Fig. 6) times the mass flow rates of that species $\dot{m}_i$ generated by the film boiling process,

$$W_P \equiv \sum_{i=1}^{n} \dot{m}_i \Delta H_{ri} \quad (21)$$

Of the six stable species detected that glycerol could be reformed into, five of them have value as a fuel: H_2, CO, CH_4, C_2H_4, and C_2H_6 so $n = 5$ in eq. (21). We do not consider CO_2 (though recent work has shown potential to convert it to methanol [30]). For Q_{in}, we use the electrical energy input to the tube which is used to decompose the gases in the film, provide the energy needed to maintain the vapor film (by evaporation of glycerol), and to compensate for thermal losses through the insulation surrounding the sealed chamber (cf, Fig. 2). Given the endothermicity of the film boiling reactor, the expectation is that $\varepsilon < 1$ as defined by eq. (20).

Using the LHVs of each species circled in Fig. 7 (H_2 and CO LHVs were computed using information given in [32]; all other LHVs were obtained from [31]) and the measured species flow rates, Fig. 8 shows the variation of ε with tube temperature. A line is included to enhance the trend. The temperatures range from the minimum film boiling temperature for glycerol (T_2 in Fig. 4) which is about 1260 K to an upper value in the experiments of 1570 K. The transformation efficiency ranges from about 20% to 50% over the temperature range of the experiments. We cannot provide a context for these values because we are unaware of previous reports of glycerol transformation efficiencies based on our definition.

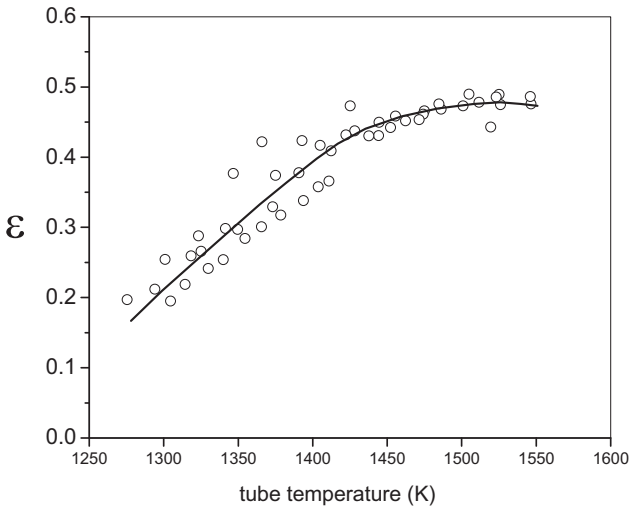

Fig. 8. Variation of ε with tube temperature.

The conversion efficiencies shown in Fig. 8 can be increased by optimizing the hardware, for example by reducing Q_{in} by minimizing heat losses from the system. In performing the experiments outlined in Section 2, we did not endeavor to optimize performance in this respect. Nonetheless, Fig. 8 shows that ε appears to saturate at around 1450 K. This is an optimal operating condition to convert glycerol into its gaseous products by film boiling, in that at higher temperatures there appears to be no further benefit to increasing the conversion efficiency. The explanation may be found in the variations of Q_{in} and W_P with temperature.

From Fig. 9, increasing Q_{in} increases the tube temperature. The glycerol evaporation rate and thereby the flow of glycerol vapor into the vapor film will increase as well. With more glycerol in the film, more of it decomposes, more products form and the product species flow rates increase. W_P then increases and so does ε. However, ε is seen to eventually level off and W_P shows signs of reaching a limit while Q_{in} continually increases. At the same time, there is another consideration on temperature's effect on W_P and ε that is hidden in Fig. 9: the effect of temperature on the residence time of gases flowing in the vapor film which also controls the conversion process.

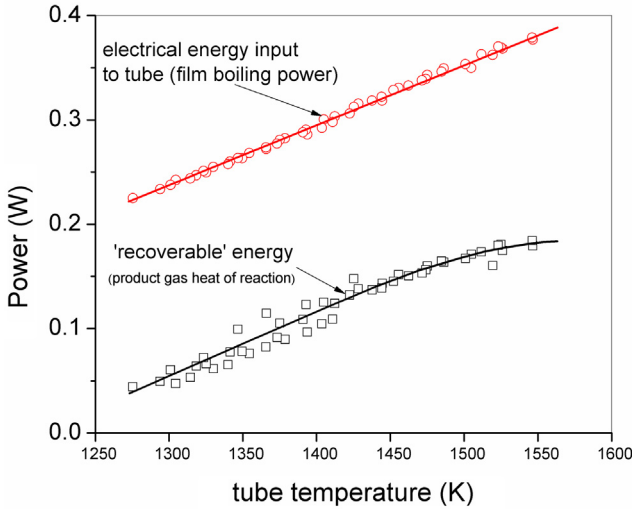

Fig. 9. Variation of W_P (Eq. (21)) and Q_{in} with tube temperature. Trend lines are shown.

It was previously shown that the residence time in the vapor film decreases with increasing tube temperature [24]. As a result, the gases in the film will be exposed to high temperatures for shorter times as the gas temperature increases compared to lower temperatures, which would ostensibly lead to lower product gas flow rates. A point is evidently reached whereby a residence time effect, on one hand, counteracts the glycerol flow and reaction rate effect on the other as temperature increases. At that point, no further increase in product flow rates and W_P is possible no matter how much electrical energy is put into the tube. ε then starts to decrease thereafter.

There is little benefit to operating film boiling as a reactor technology at temperatures higher than the peak shown in Fig. 8 because the transformation efficiency decreases thereafter. As a final point, the efficiency values shown in Fig. 8 are specific to the particular experimental design of Fig. 2 though the physics of operation noted above should be more broadly applicable.

5. Conclusions

A chemical processing technology has been described based on film boiling to transform glycerol into a combustible gaseous mixture. It was found that the total product gas flow rate increases with temperature. The predominant non-condensable product species detected in the exhaust stream are synthesis gas while along with smaller amounts of CH_4, C_2H_4, CO_2, and C_2H_6. Approximately 95% of the products are combustible gases with 72% consisting of syngas at all temperatures examined.

The presence of stable species other than syngas suggests a more complicated decomposition process than unimolecular. A set of reactions based on sensitivity and pathway analysis are identified as most probable to explain the species detected in the experiments. The pathway analysis shows that the decomposition of glycerol proceeds through the initiation reactions producing 3-hydroxypropanal and acetol, followed by propagation reactions that produce intermediates. These intermediates finally produce the stable product gases detected in the experiments.

An operating condition is identified in terms of a tube temperature above which the product yields do not continue to increase with temperature. This peak was considered to arise from a competition between the reaction and evaporate rates of glycerol into the film and residence time of the gases in the film.

The results presented are consistent with more conventional reactor designs thus showing the potential for film boiling as a viable method to transform glycerol as a waste product of biodiesel production into more useful gaseous products.

Declaration of Competing Interest

The authors declared that there is no conflict of interest.

Acknowledgements

This study was supported by grant no. 1336657 from the US National Science Foundation, United States with Dr. Jose L. Lage as the program manager. The authors also thank Drs. Sumanta Acharya of the Illinois Institute of Technology, Alfonso Ortega of Villanova University and Theodore Bergman of the University of Kansas for their interest. The assistance of Dr. Ivan Keresztes of the Cornell Department of Chemistry and Chemical Biology in analyzing the composition of the liquid pool is much appreciated.

Appendix A

Converting flow meter output (in volts, V) to flow rates requires calibrating the flow meter for the individual species expected in the product stream. Calibration curves were developed for H_2, CO, CH_4, CO_2, C_2H_4, and C_2H_6. An absolute standard flow meter (Bios International Corp., Definer 220) was used to obtain flow rates in units of ml/min.

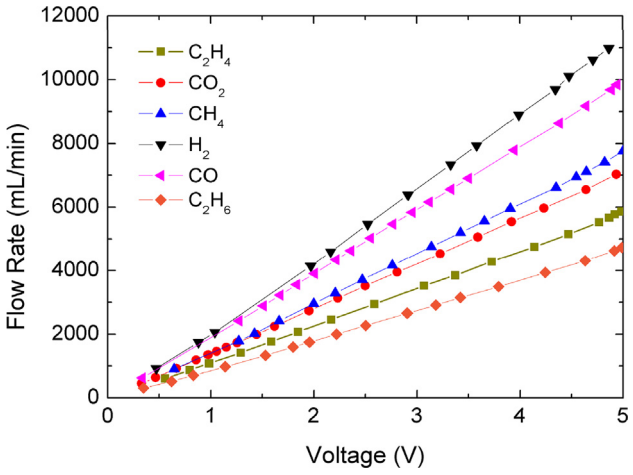

Fig. A1. Calibration curve (Eq. A1) of flow meter FMA-A2309 for the gases detected in the glycerol decomposition product stream.

Table A1
Correlation coefficients (Eq. A1).

Coefficients	H_2	CO	CO_2	CH_4	C_2H_4	C_2H_6
A_{oi}	−147.49	−77.058	−8.7361	−119.72	−14.442	−22.164
A_{1i}	2130.3	1981.3	1384.6	1516.4	1101.8	872.82
A_{2i}	33.782	3.7927	7.4399	9.7132	13.839	14.829

Gases from separate cylinders were passed through the flow meter and the output (in volts) recorded. Fig. A1 shows the resulting calibration curves for the individual volumetric flow rates $\dot{m}_i$. The curves are nearly linear though a quadratic equation was fitted to the data for a slightly more accurate correlation,

$$\dot{m}_i = A_{oi} + A_{1i}V + A_{2i}V^2 \tag{A1}$$

The coefficients in Eq. (A1) are given in Table A1.

The total volumetric flow rate shown in Fig. 5 involves all of the (six) gases in the product stream and is expressed as

$$\dot{m} = \sum_{i=1}^{6} \chi_i \dot{m}_i \tag{A2}$$

where χ_i and $\dot{m}_i$ are the mole fraction and volumetric flow rates of the i-th species in the mixture, respectively. The mole fractions are obtained from GC analysis of the exhaust gases as noted in Section 2.

Appendix B

This appendix describes the general procedure to convert GC outputs to species and fractional amounts in the gas mixture. The processes noted below are standard though repeated here for completeness.

Approximately 30 mL/min of the product gas output from the chamber in Fig. 2 was directed to the GC, a series-600-TCD GC from Gow-Mac Instruments. There are two columns inside the GC: a Molecular Sieve 13x, for detecting H_2, O_2, N_2, CH_4, and CO; and a Haysep Q suitable for detecting N_2, O_2, CH_4, CO_2, C_2H_4, C_2H_2, C_2H_6, C_3H_8, H_2S, and N_2O. O_2 and N_2 were not considered for this particular analysis.

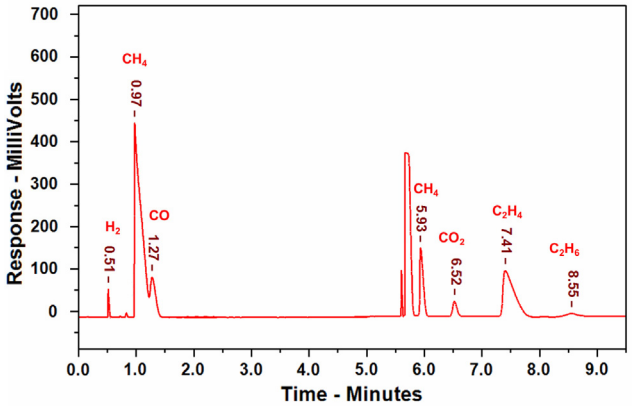

Fig. A2. A sample chromatogram obtained from the Chromperfect software. Each peak corresponds to one gaseous component which can be figured out by comparing the retention time with its calibration data (Fig. A1). The mole percentage of each species can be evaluated comparing its peak area to its calibration data.

The gas stream is passed through the first column for five minutes then switched to the second column for 10 min. The actuator and carrier gases were nitrogen and helium, respectively. The oven and thermal conductivity detector temperatures were kept at 60 °C and 100 °C, respectively. The GC was controlled by the Chromperfect software. A sample output of GC response from the software is shown in Fig. A2, which corresponds to the product stream gases (details are discussed below). There are two important parts of GC analysis: calibration and final measurement of different unknown components from the product stream.

For the calibration, individual pure gases were used separately to find their peaks and respective properties. The software provides all the individual peak properties (e.g., the peak area, width, retention time, etc.). These properties are combined to form the overall calibration data. As each individual pure gas was used for calibration, their corresponding chromatograms contain only one peak (as opposed to multiple peaks in Fig. A2). The area under these singular peaks represent a unity mole fraction. The only exception is CH_4, for which the chromatogram contains two peaks, as it is detected by both columns.

When the product gas stream is passed through both columns at each power input step, a chromatogram with multiple peaks is generated (e.g., Fig. A2, with each peak corresponding to one of the gaseous species). The individual peak properties were collected from the software. The retention times and peak areas were compared to the calibration data to determine which peaks correspond to which species and the molar percentage of each species. The first two peaks in the second column were ignored from the analysis because they corresponded to N_2 and O_2. From the first column part of Fig. A2, it is evident that two peaks (CH_4 and CO) are merged. To ensure proper measurements, CH_4 percentage was measured from the second column and only CO was measured from that merged peak. Table 1 shows the molar percents of the indicated species at three temperatures.

References

[1] J.C. Thompson, B.B. He, Characterization of crude glycerol from biodiesel production from multiple feedstocks, Appl. Eng. Agric. 22 (2006) 261–265.
[2] R. Ciriminna, C. Della Pina, M. Rossi, M. Pagliaro, Understanding the glycerol market, Eur. J. Lipid Sci. Technol. 116 (2014) 1432–1439.
[3] M. Pagliaro, R. Ciriminna, H. Kimura, M. Rossi, C. Della Pina, From glycerol to value-added products, Angew. Chem. Int. Ed. 46 (2007) 4434–4440.
[4] D. Nilles, Combating the glycerin glut, Biodiesel Mag. (2006). http://www.biodieselmagazine.com/articles/1123/combating-the-glyce.
[5] C.A. Quispe, C.J. Coronado, J.A. Carvalho Jr, Glycerol: production, consumption, prices, characterization and new trends in combustion, Renew. Sustain. Energy Rev. 27 (2013) 475–493.
[6] M. Angeloni, P. Remacha, A. Martínez, J. Ballester, Experimental investigation of the combustion of crude glycerol droplets, Fuel 184 (2016) 889–895.
[7] S.J. Eaton, G.N. Harakas, R.W. Kimball, J.A. Smith, K.A. Pilot, M.T. Kuflik, J.M. Bullard, Formulation and combustion of glycerol–diesel fuel emulsions, Energy Fuels 28 (2014) 3940–3947.
[8] M.D. Bohon, B.A. Metzger, W.P. Linak, C.J. King, W.L. Roberts, Glycerol combustion and emissions, Proc. Combust. Inst. 33 (2011) 2717–2724.
[9] C.R. Coronado, J.A. Carvalho, C.A. Quispe, C.R. Sotomonte, Ecological efficiency in glycerol combustion, Appl. Therm. Eng. 63 (2014) 97–104.
[10] L. Jiang, A.K. Agrawal, Combustion of straight glycerol with/without methane using a fuel-flexible, low-emissions burner, Fuel 136 (2014) 177–184.
[11] J. McNeil, P. Day, F. Sirovski, Glycerine from biodiesel: the perfect diesel fuel, Process Saf. Environ. Prot. 90 (2012) 180–188.
[12] P. Queirós, M. Costa, R. Carvalho, Co-combustion of crude glycerin with natural gas and hydrogen, Proc. Combust. Inst. 34 (2013) 2759–2767.
[13] S. Adhikari, S.D. Fernando, A. Haryanto, Hydrogen production from glycerin by steam reforming over nickel catalysts, Renew. Energy 33 (2008) 1097–1100.
[14] T. Valliyappan, N. Bakhshi, A. Dalai, Pyrolysis of glycerol for the production of hydrogen or syn gas, Bioresour. Technol. 99 (2008) 4476–4483.
[15] I.N. Buffoni, F. Pompeo, G.F. Santori, N.N. Nichio, Nickel catalysts applied in steam reforming of glycerol for hydrogen production, Catal. Commun. 10 (2009) 1656–1660.
[16] B. Dou, Y. Song, C. Wang, H. Chen, Y. Xu, Hydrogen production from catalytic steam reforming of biodiesel byproduct glycerol: issues and challenges, Renew. Sustain. Energy Rev. 30 (2014) 950–960.
[17] J.M. Encinar, J.F. González, G. Martínez, N. Sánchez, I.M. Sanguino, Hydrogen production by means pyrolysis and steam gasification of glycerol, presented at Int, Conf. on Renewable Energies and Power Quality, Las Palmas de Gran Canaria, Spain, 2011.
[18] S.M. Kim, S.I. Woo, Sustainable production of syngas from biomass-derived glycerol by steam reforming over highly stable Ni/SiC, ChemSusChem 5 (2012) 1513–1522.
[19] M.R. Nanda, Y. Zhang, Z. Yuan, W. Qin, H.S. Ghaziaskar, C.C. Xu, Catalytic conversion of glycerol for sustainable production of solketal as a fuel additive: a review, Renew. Sustain. Energy Rev. 56 (2016) 1022–1031.
[20] A.P.G. Peres, D.R. de Lima, N.D. da Silval, M.R.W. Maciel, Syngas production and optimization from glycerol pyrolysis, Chem. Eng. Trans. 20 (2010) 333–338.
[21] R.R. Soares, D.A. Simonetti, J.A. Dumesic, Glycerol as a source for fuels and chemicals by low-temperature catalytic processing, Angew. Chem. Int. Ed. 118 (2006) 4086–4089.
[22] Y.S. Stein, M.J. Antal, M. Jones, A study of the gas-phase pyrolysis of glycerol, J. Anal. Appl. Pyrol. 4 (1983) 283–296.
[23] F. Bauer, C. Hulteberg, Isobutanol from glycerine – a techno-economic evaluation of a new biofuel production process, Appl. Energy 122 (2014) 261–268.
[24] C.T. Avedisian, W.C. Kuo, W. Tsang, A. Lowery, High temperature thermal decomposition of diethyl carbonate by pool film boiling, J. Heat Transfer 140 (2018) 061501.
[25] C.T. Avedisian, W.C. Kuo, W. Tsang, A. Lowery, A film boiling study of ethanol pyrolysis, Ind. Eng. Chem. Res. 57 (2018) 8334–8340.
[26] J.H. Lienhard IV, J.H. Lienhard V, in: A Heat Transfer Textbook, third ed., Phlogiston, Cambridge, MA, 2003, pp. 483–484, http://ahtt.mit.edu.
[27] V.P. Carey, Liquid-Vapor Phase Change Phenomena, Taylor & Francis, 1992, p. 252.
[28] E.B. Hemings, C. Cavallotti, A. Cuoci, T. Faravelli, E. Ranzi, A detailed kinetic study of pyrolysis and oxidation of glycerol (propane-1, 2, 3-triol), Combust. Sci. Technol. 184 (2012) 1164–1178.
[29] A.D. Stepukhovich, V.M. Umanskii, Kinetics and mechanism of three-body recombination of atoms and radicals, Russ. Chem. Rev. 38 (8) (1969) 590–607.
[30] I. Ganesh, Conversion of carbon dioxide into methanol – a potential liquid fuel: fundamental challenges and opportunities, Renew. Sustain. Energy Rev. col. 31 (2014) 221–257.
[31] P.J. Linstrom, W.G. Mallard, NIST Chemistry WebBook, NIST Standard Reference Database Number 69, Eds. National Institute of Standards and Technology, Gaithersburg MD, 20899, doi: 10.18434/T4D303, address: https://webbook.nist.gov/chemistry/.
[32] S.R. Turns, An Introduction to Combustion, First Ed., McGraw-Hill; New York, NY, 1996, pp. 514–541.